Check for updates

Advanced Science

ADVANCED SCIENCE Open Access

www.advancedscience.com

RESEARCH ARTICLE OPEN ACCESS

A Renal Clearable Probe for In Vivo Monoamine Oxidase (MAO) Detection

Marcia Domínguez[1,2] | David Azorín-Soriano[1,3] | Araceli Lérida-Viso[1,2,3,4] | Jessie García-Fleitas[1,2] | Paula M Soriano-Teruel[1,2,3,4] | Jennifer Soler Beatty[1,3,4] | Paula Rodrigo-Martínez[5] | Pau Arroyo[5,6] | Sara Rojas-Vázquez[1,2,7] | Isabel Fariñas[7,8] | Félix Sancenón[1,2,3,4] | Juan F. Blandez[1,4,9] | Alba García-Fernández[1,2,3,4] | Ramón Martínez-Máñez[1,2,3,4]

[1]Instituto Interuniversitario de Investigación de Reconocimiento Molecular y Desarrollo Tecnológico (IDM), Universitat Politècnica de València, Universitat de València, Valencia, Spain | [2]CIBER de Bioingeniería, Biomateriales y Nanomedicina (CIBER-BBN), Instituto de Salud Carlos III, Madrid, Spain | [3]Unidad Mixta UPV-CIPF de Investigación en Mecanismos de Enfermedades y Nanomedicina, Universitat Politècnica de València, Centro de Investigación Príncipe Felipe, Valencia, Spain | [4]Unidad Mixta de Investigación en Nanomedicina y Sensores, Universitat Politècnica de València, Avenida Fernando Abril Martorell, Instituto de Investigación Sanitaria La Fe (IIS La Fe), Valencia, Spain | [5]Instituto Interuniversitario de Investigación de Reconocimiento Molecular y Desarrollo Tecnológico, Universitat de València, Universitat Politècnica de València, Burjassot, Valencia, Spain | [6]Departamento de Química Orgánica, Universitat de València, Burjassot, Valencia, Spain | [7]Instituto de Biotecnología y Biomedicina (BIOTECMED), Universitat de València, Valencia, Spain | [8]CIBER de Enfermedades Neurodegenerativas (CIBERNED), Instituto de Salud Carlos III, Madrid, Spain | [9]Instituto de Ciencia Molecular (ICMol), Universidad de Valencia, Paterna, Valencia, Spain

Correspondence: Alba García-Fernández (algarfe4@etsiamn.upv.es) | Ramón Martínez-Máñez (rmaez@qim.upv.es)

Received: 22 December 2025 | **Revised:** 4 February 2026 | **Accepted:** 6 February 2026

Keywords: monoamine oxidase | non-invasive tool | renal clearable probe | zwitterionic compounds

ABSTRACT

Hyperactivation of monoamine oxidase enzymes (MAO) is associated with uncontrolled production of neurotoxic compounds such as reactive oxygen species, whose accumulation is linked to neurodegenerative, chronic, and age-related diseases. Although chromo-fluorogenic probes for detecting and quantifying MAO activity have been reported, non-invasive methods for monitoring MAO overexpression in vivo remain elusive. Here, we report a renal-clearable fluorogenic probe based on the cyanine-7 fluorophore (**Cy7-MAO**) for in vivo detection of MAO overexpression through a simple measurement of the fluorescence in urine. The probe incorporates sulfonic acid moieties for renal clearance and a propylamino group as a MAO substrate. Upon administration, **Cy7-MAO** is hydrolysed at the site by MAO, releasing a highly emissive Cy7 fluorophore, which is excreted in urine and quantified by fluorescence. **Cy7-MAO** is validated in vitro using HepG2 liver human cells, which express elevated MAO levels. We further demonstrate the in vivo applicability of **Cy7-MAO** for MAO activity monitoring in aged mice, which show significantly higher urine fluorescence than young mice, consistent with an elevated MAO activity in older animals. These findings support **Cy7-MAO** as a tool for longitudinal assessment of MAO activity in vivo, providing a novel approach to study MAO-related pathologies.

1 | Introduction

Early and precise detection is crucial for effective diagnosis and treatment across a wide range of pathologies. Traditional diagnostic techniques, such as Magnetic Resonance Imaging (MRI), Positron Emission Tomography (PET), and Computed Tomography (CT), although widely used, have several limitations [1–4]. These include high costs, the need for specialised equipment

This is an open access article under the terms of the Creative Commons Attribution License, which permits use, distribution and reproduction in any medium, provided the original work is properly cited.

© 2026 The Author(s). *Advanced Science* published by Wiley-VCH GmbH

and trained personnel, and, in some cases, the administration of contrast agents that can cause adverse effects. Moreover, many other biomarker detection methods suffer from limited specificity and accumulation in tissues, increasing the risk of toxicity. In response to these challenges, the design of non-invasive and cost-effective diagnostic protocols is gaining significant interest. Urine-based detection platforms represent a significant advancement, facilitating the identification of biomarkers and providing a robust complement or, in certain contexts, an alternative to conventional bioimaging modalities [5, 6].

A particularly innovative approach in the development of urine diagnostic tools is the preparation of probes that produce highly emissive fluorophores, which are subsequently excreted in urine. In this approach, an OFF-state probe is transformed into a highly emissive ON-state fluorophore by the action of a specific cellular biomarker. Moreover, the fluorophore is designed for rapid renal clearance, meaning it passes through the kidneys to reach the bladder for excretion in urine, enabling easy fluorescence detection in urine. Based on this mechanism, biomarkers can be detected via urinalysis, a technique that has been proven as a valuable tool for diagnosing and monitoring various medical conditions [7]. Recent studies have expanded on this concept, employing protease-responsive nanoparticles [8, 9], fluorescent or chemiluminescent derivatives functionalized with β-cyclodextrin (HPβCD) [10, 11], and other renal-clearable organic molecular probes. Among the latter are hemicyanine-based fluorophores conjugated to HPβCD or dextran backbones for detecting biomarkers such as Caspase-3 [7], gamma-glutamyl transferase [12], and SARS-CoV-2 [13]. In this context, we have also recently reported a probe that allows simple and semi-quantitative assessment of senescence burden in vivo [5]. These examples represent the first reports of fluorogenic probes capable of detecting target biomarkers by urine analysis, highlighting the potential of renally activatable probes as accessible and clinically translatable diagnostic tools. Their ability to monitor biomarker dynamics longitudinally represents a distinct advantage for geriatric applications, where minimally invasive measurements are highly valuable. In addition, rapid elimination through urine minimizes tissue accumulation and potential toxicity. Encouraged by these promising results, we decided to extend this strategy to other clinically relevant biomarkers for which non-invasive detection methods have not yet been fully developed.

Monoamine oxidase (MAO) enzymes represent a particularly compelling target due to their central role in neurotransmitter metabolism and the generation of hydrogen peroxide (H_2O_2) and other reactive oxygen species (ROS). These flavoenzymes are located on the outer mitochondrial membrane and can be found in most cell types in the body. MAO enzymes exist in two isoforms, MAO-A and MAO-B, which share a 70% sequence homology but different substrate and inhibitor specificities [14]. MAO-A mainly cleaves serotonin, melatonin, noradrenaline, and adrenaline, while MAO-B acts on phenethylamine and benzylamine [15]. During the oxidative deamination of these substrates, MAO activity produces H_2O_2 and other ROS as byproducts [16–19]. Tissue-specific changes in MAO levels have been described in age-related disorders, as increased oxidative stress and mitochondrial dysfunction are key factors in cellular and organ function [20, 21]. For instance, the accumulation of ROS has been implicated in the pathogenesis of several neurodegenerative diseases, including Parkinson, Alzheimer or amyotrophic lateral sclerosis [22–25], as well as chronic conditions such as endothelial dysfunction in hypertension, metabolic disorders, and chronic kidney disease [26, 27]. Many of these chronic conditions are highly prevalent in aging populations and contribute to the functional decline associated with aging [28].

Despite the involvement of MAO enzymes in various pathological and age-related conditions, tools to monitor tissue-specific changes in MAO in vivo are extremely limited or non-existent. Several procedures have been described in the literature to detect MAO overexpression, such as Enzyme-Linked Immunosorbent Assay (ELISA), High Performance Liquid Chromatography (HPLC), or spectrophotometric assays [29–31]. However, these approaches frequently rely on terminal procedures, such as tissue extraction or cell lysis, which preclude longitudinal measurements. As a result, their utility is largely confined to in vitro and ex vivo detection, with only limited instances successfully applied to in vivo monitoring (Table S1) [32–34]. Moreover, many probes rely on conventional fluorophores with poor aqueous solubility, low quantum yield in biological environments, or non-specific background fluorescence and limited elimination. In this scenario, renal-clearable OFF–ON fluorescent probes emerge as a promising alternative for in vivo dynamic monitoring of MAO activity.

We report herein a fluorescent molecular probe, **Cy7-MAO**, based on a cyanine-7 fluorophore containing a propylamine group as recognition moiety (Figure 1a) [35–40]. The sensing mechanism is based on an increase in fluorescence signal in the presence of MAO enzymes, which transform the weakly emissive **Cy7-MAO** molecule into the high-emissive Cy7 fluorophore. To achieve urinalysis, the probe backbone contains two sulfonic acid groups to enhance solubility and promote rapid renal clearance in vivo (Figure 1b), while the zwitterionic nature of the probe is also expected to reduce non-specific protein binding and uptake by healthy tissues [5, 41, 42]. In this context, **Cy7-MAO** provides a robust and versatile approach, enabling, for the first time, non-invasive, longitudinal monitoring of MAO activity in living animals via urine collection. This design not only functions in vitro and ex vivo but also fills a critical gap in MAO research, providing unique biological insight into enzyme dynamics.

2 | Results and Discussion

2.1 | Synthesis and characterisation of Cy7-MAO probe

Cy7-MAO was synthesized by a two-step procedure (Figure 2a). In a first step, a nucleophilic substitution reaction between BOC-protected 3-bromopropylamine and 5-formylsalycilaldehyde was carried out, and the BOC-protecting group was removed with TFA, yielding the intermediate compound **1**. Then, in a second step, a Knoevenagel condensation between **1** and 2,3,3-trimethyl-1-(4-sulfobutyl) indolium (**2**) yielded the final **Cy7-MAO** probe. **Cy7-MAO** was purified by silica gel chromatography and fully characterized by ^{1}H-NMR, ^{13}C-NMR, and HRMS (Figures S1–S5). In addition, the Cy7 fluorophore was synthesized according to previously reported procedures (Figure S6) [5]. On the other hand, emission of Cy7 fluorophore solutions (20 μM in HEPES,

21983844, 2026, 23, Downloaded from https://advanced.onlinelibrary.wiley.com/doi/10.1002/advs.202520797 by Spanish Cochrane National Provision (Ministerio de Sanidad), Wiley Online Library on [24/04/2026]. See the Terms and Conditions (https://onlinelibrary.wiley.com/terms-and-conditions) on Wiley Online Library for rules of use; OA articles are governed by the applicable Creative Commons License

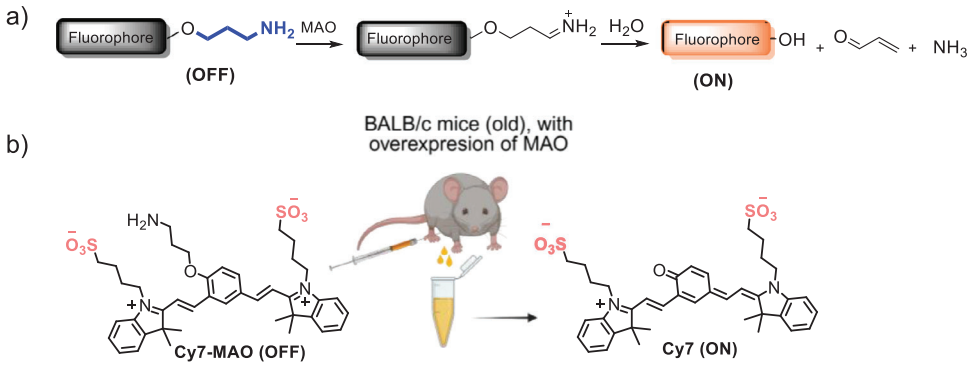


FIGURE 1 | Design and performance of **Cy7-MAO** probe. (a) Schematic illustration of the activatable OFF-ON fluorescence probe for the detection of MAO enzymes. (b) Structure of the fluorescent probe **Cy7-MAO** and the product Cy7 after catalytic oxidative deamination by MAO enzymes.

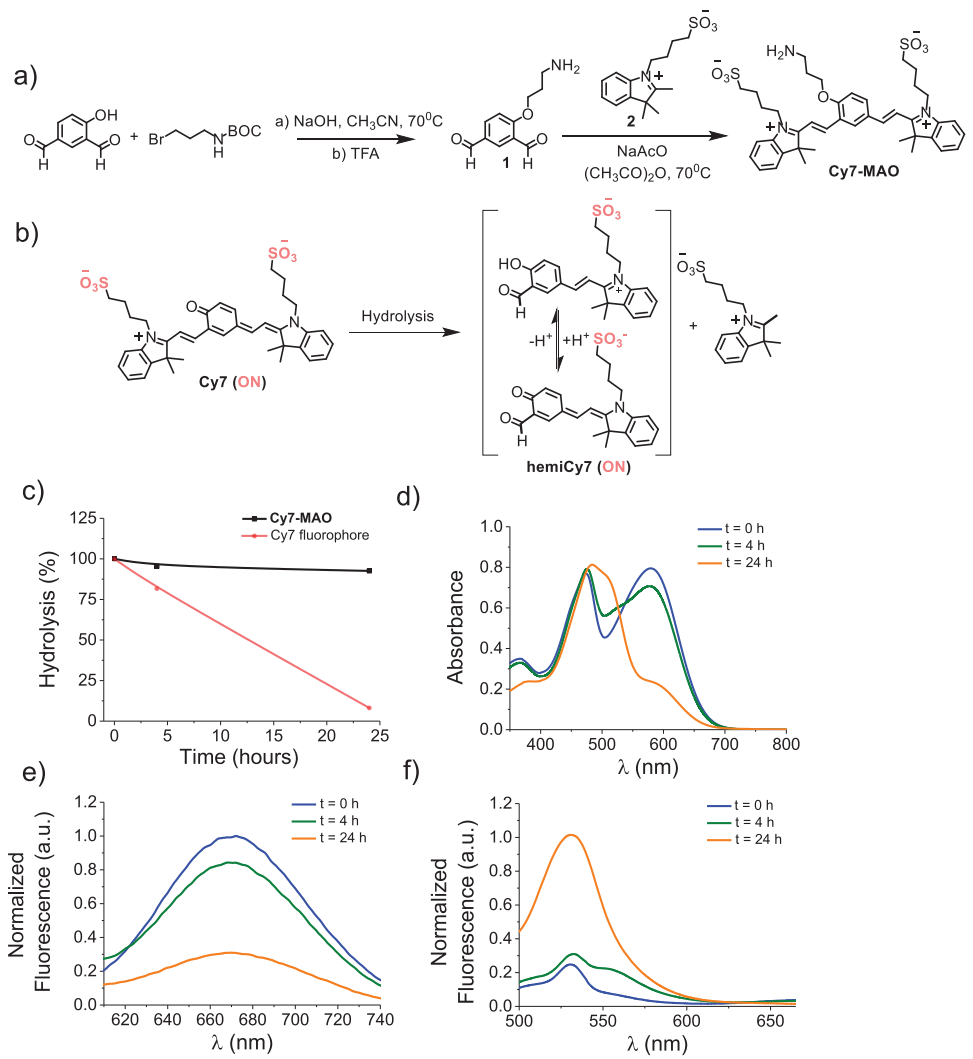


FIGURE 2 | Synthesis and mechanistic studies of **Cy7-MAO** hydrolysis. (a) Synthetic sequence to prepare **Cy7-MAO**. (b) Hydrolysis of the Cy7 fluorophore. (c) % hydrolysis of **Cy7-MAO** and Cy7 vs. time. The stability study was carried out by HPLC-MS using an eluent gradient method from H_2O-acetonitrile (100:0 v/v) to H_2O-acetonitrile (0:100 v/v) at 20 min with a flow rate of 0.4 mL·min^{-1} with a kromasil C18 column. Mass spectroscopy chromatograms were recorded with an Agilent Ultivo mass spectrometer equipped with a triple Q-TOF detector using a dual selected ion monitoring (SIM) function at 745 m/z and 705 m/z simultaneously, corresponding to the **Cy7-MAO** and Cy7 fluorophore, respectively. (d) Absorption spectra of the Cy7 fluorophore (10^{-4} M in HEPES (10 mM, pH 7.4)) at different time points. (e), (f) Fluorescence emission spectra of the Cy7 fluorophore (10^{-4} M in HEPES (10 mM, pH 7.4)) at different time points, using excitation wavelengths at 580 nm (e) and 450 nm (f).

21983844, 2026, 23, Downloaded from https://advanced.onlinelibrary.wiley.com/doi/10.1002/advs.202520797 by Spanish Cochrane National Provision (Ministerio de Sanidad), Wiley Online Library on [24/04/2026]. See the Terms and Conditions (https://onlinelibrary.wiley.com/terms-and-conditions) on Wiley Online Library for rules of use; OA articles are governed by the applicable Creative Commons License

10 mM, pH 7.4) at different pH values corroborated fluorophore stability (in short periods of time) in the 5–10 pH range (Figure S7).

Cy7 fluorophore presents remarkable photophysical features for bioimaging (NIR emission), but its use in biological media requires careful evaluation as it can be hydrolyzed into a hemicyanine aldehyde (hemiCy7, see Figure 2b), which is also emissive [41]. In order to assess the applicability of the **Cy7-MAO** probe, its stability together with that of Cy7 was tested through HPLC-MS studies (Figure 2c; Figures S8 and S9). For this purpose, solutions of **Cy7-MAO** and Cy7 (10^{-4} M in 10 mM HEPES, pH 7.4) were prepared, and mass spectrometry chromatograms were recorded using a mass spectrometer equipped with a triple Q-TOF detector, which employed a dual selected ion monitoring (SIM) function at 745 m/z (**Cy7-MAO** probe) and 705 m/z (Cy7 fluorophore) simultaneously. Mass spectra, at both m/z ratio, were recorded at different times, and the results obtained are depicted in Figure 2c. As could be seen, after 24 h, the abundance of the molecular ion selected to monitor the presence of the **Cy7-MAO** (745 m/z corresponding to $[M\text{-}CH_3]^+$) remained unchanged, whereas that of the Cy7 fluorophore (705 m/z corresponding to $[M+H]^+$) drastically decreased (ca. 92%). This disappearance was associated with the hydrolysis of the Cy7 fluorophore to hemiCy7 (Figure 2b).

UV-vis measurements also confirmed the proposed hydrolysis process (Figure 2d). HEPES solutions of Cy7 fluorophore showed a marked absorption band centered at ca. 600 nm which gradually decreased with time, while a new band appeared at ca. 450 nm, ascribed to hemiCy7 that was formed after Cy7 hydrolysis. The same results were obtained using fluorescence measurements (Figure 2e,f). Thus, upon excitation at 580 nm, the characteristic emission of Cy7 fluorophore at ca. 670 nm was observed (Figure 2e). However, this emission band was progressively reduced until it almost disappeared after 24 h. As a clear contrast, under excitation at 450 nm (absorption of hemiCy7), an emission band was found at ca. 535 nm after 24 h. These studies corroborate the formation of hemiCy7 after hydrolysis of Cy7. To corroborate these observations, hemiCy7 was also synthesized [43] and characterized by NMR, as well as by optical spectroscopic techniques, including UV-vis absorption and fluorescence spectroscopy (Figures S10 and S11). These studies validate the proposed hydrolysis pathway and confirm the identity of the product resulting from the hydrolysis of Cy7. Despite the inherent instability of the Cy7 fluorophore at long time, the results also confirm that the **Cy7-MAO** probe remains chemically stable in aqueous buffer at physiological pH. This stability supports its potential utility in biological applications, such as the detection of elevated MAO levels without degradation.

2.2 | Selective MAO detection using the Cy7-MAO probe

Cy7-MAO was photophysically studied under simulated physiological conditions in the presence or absence of MAO-A or MAO-B enzymes. In a typical experiment, **Cy7-MAO** (5 μM) in HEPES solution (10 mM, pH 7.4) was mixed with MAO-A or MAO-B (0–100 $\mu g \cdot mL^{-1}$) and the mixture was incubated at 37°C for 24 h to allow a complete enzyme-mediated oxidative deamination of the probe. Emission after 24 h was measured at 535 nm (λ_{ex} = 450 nm) that is the emission of the hemiCy7 derivative obtained by hydrolysis of Cy7 after this time (*vide ante*). Starting **Cy7-MAO** (5 μM) solutions in HEPES (10 mM, pH 7.4) were weakly emissive upon excitation at 450 nm, whereas, in sharp contrast (Figure 2a), a broad fluorescence band centered at 535 nm was observed upon addition of both enzymes (at 100 $\mu g \cdot mL^{-1}$) after 24 h (13.2- and 9.7-fold emission enhancement for MAO-A and MAO-B, respectively). Next, the fluorescence emission of **Cy7-MAO** probe (5 μM) was monitored after 24 h in the presence of different amounts of MAO-A or MAO-B (0–100 $\mu g \cdot mL^{-1}$) (Figure 3c,e). A significant increase in emission at 535 nm, proportional to the amount of enzyme added was found. These data were used to determine the LOD and LOQ for both enzymes (Figure 3d,f). LOD of 6.4 and 10.9 $\mu g \cdot mL^{-1}$ and LOQ values of 29.3 and 52.1 $\mu g \cdot mL^{-1}$ were found for MAO-A and MAO-B, respectively. These results indicate that the **Cy7-MAO** probe can be used for the qualitative and quantitative detection of both MAO isoforms.

To further characterize its enzymatic behaviour, the kinetics of the reactions between **Cy7-MAO** and MAO-A and MAO-B were investigated (Figure S12). The Michaelis–Menten analysis yielded the following catalytic parameters: for MAO-A, a maximum velocity (V_{max}) of 16.13 $\mu M \cdot min^{-1}$ and a Michaelis constant (K_m) of 10.63 μM; for MAO-B, a V_{max} of 35.71 $\mu M \cdot min^{-1}$ and a K_m of 17.82 μM. The lower K_m for MAO-A indicates a higher apparent affinity of **Cy7-MAO** for this isoform. In contrast, the higher V_{max} for MAO-B reflects a greater catalytic capacity under substrate-saturating conditions. These results demonstrate that **Cy7-MAO** is efficiently recognised and processed by both MAO isoforms, albeit with distinct kinetic profiles, confirming its suitability as a sensitive and reliable probe for monitoring MAO activity. Taken together, these data provide strong experimental support for the use of **Cy7-MAO** in enzymatic studies targeting both MAO-A and MAO-B.

To investigate and gain insights into the binding orientation and molecular interactions between **Cy7-MAO** and the MAO-A and MAO-B isoforms, molecular docking studies (MD) were performed using the AutoDock Tools platform (MGL Tools suite v1.5.7). The results of the MD analysis showed that the ligand fits into the active site cavity of both isoforms. In some of the resulting clusters, the amino group-containing end of **Cy7-MAO** is seen to be close to the FAD cofactor, which is naturally present in MAO enzymes. The most promising complex of MAO-A and MAO-B with **Cy7-MAO**, based on binding energy and more populated clusters, was subjected to stability analysis using MD simulations of 200 ns. The results of the simulations showed that the complexes with the two isoforms were stable during the simulation time, with the side chain containing the amino moiety remaining in the vicinity of FAD, which is stated as the catalytic site of the enzyme. The RMSD graph (Figure S13a) for MAO-A in complex with **Cy7-MAO** shows that the system stabilizes before 50 ns and subsequently remains stable with very little fluctuation. These values indicate that the complex exhibits good stability. In the case of MAO-B in complex with **Cy7-MAO** (Figure S13b), similar behavior is observed, with rapid stabilization of the system and subsequent small fluctuations.

21983844, 2026, 23, Downloaded from https://advanced.onlinelibrary.wiley.com/doi/10.1002/advs.202520797 by Spanish Cochrane National Provision (Ministerio de Sanidad), Wiley Online Library on [24/04/2026]. See the Terms and Conditions (https://onlinelibrary.wiley.com/terms-and-conditions) on Wiley Online Library for rules of use; OA articles are governed by the applicable Creative Commons License

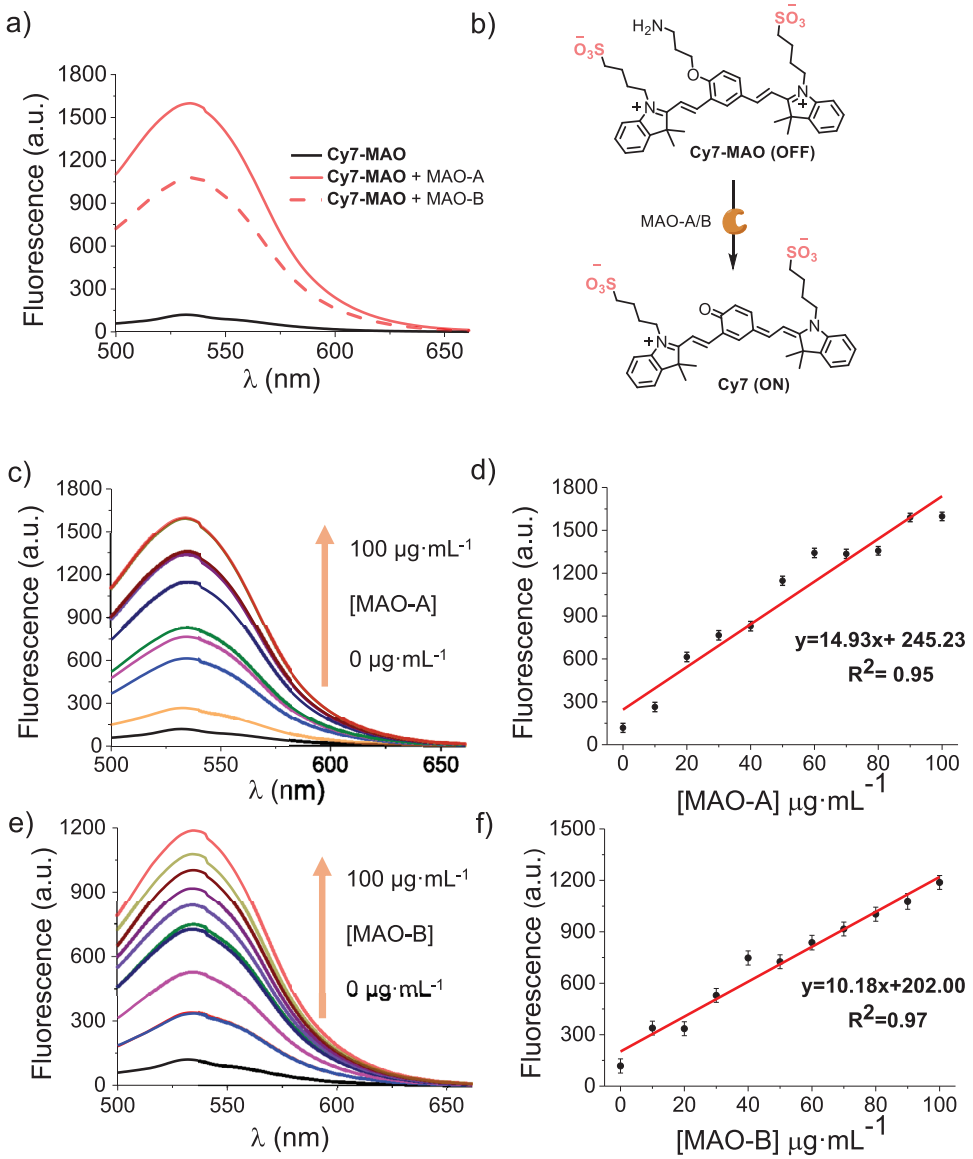


FIGURE 3 | MAO-mediated activation of **Cy7-MAO**. (a) Fluorescence emission spectra (λ_{exc} = 450 nm) of **Cy7-MAO** (5 μM) (black curve) and **Cy7-MAO** (5 μM) + MAO-A/B (100 μg·mL^{-1}) (orange curves) in HEPES (10 mM, pH 7.4) after 24 h of incubation at 37°C. (b) MAO-induced oxidative deamination of **Cy7-MAO**. (c), (e) Fluorescence spectra of **Cy7-MAO** (5 μM) in the presence of increasing MAO-A/B concentrations (0–100 μg·mL^{-1}) after 24 h of incubation at 37°C. (d), (f) Calibration curve of **Cy7-MAO** for MAO-A/B in HEPES solution (10 mM, pH 7.4). Error bars are expressed as 3σ from three independent experiments.

The MD simulations indicate there is little movement at both binding sites, and a representative binding mode for **Cy7-MAO** in complex with MAO-A can be seen in Figure 4a, while the one with MAO-B is shown in Figure 4b. In both cases, the amino group of **Cy7-MAO** is facing the N5 and the carbonyl group of the FAD catalytic site. One reason for the stabilization of the probe in the active site cavity is most likely related to the presence of two Tyr residues that form an aromatic cage. In the case of MAO-A, these are Tyr433 and Tyr396 (Figure S14a), and in the case of MAO-B, Tyr434 and Tyr397 (Figure S14b). The results of the computer simulation agree with the experimental results and help explain how **Cy7-MAO** binds to the MAO-A and MAO-B isoforms of the enzyme for the catalytic oxidation of the monoamine in **Cy7-MAO** to give Cy7.

The selectivity of **Cy7-MAO** probe to detect MAO-A and MAO-B was also assessed in the presence of several potentially interfering species [44]. As showed in Figure 4c, only both MAO isoforms induced a remarkable emission enhancement in **Cy7-MAO**, whereas no changes were found in the presence of selected ions (Na^+, K^+, NO_3^-, Ca^{2+}, Mg^{2+}, Fe^{2+}, Fe^{3+}), small molecules (H_2O_2, vitamin C, arginine, urea, glucose, glutathione, L-Histidina, L-Glutamic acid) or other enzymes (acetyl cholinesterase, leucine aminopeptidase, β-galactosidase, phosphatase, esterase, DNase, glucose oxidase). Besides, additional experiments were performed in the presence of MAO enzymes and the MAO inhibitors clorgyline for MAO-A and pargyline for MAO-B [24, 45]. In both cases, the fluorescence signal in the presence of inhibitors was 70% lower than the signal in its absence,

21983844, 2026, 23, Downloaded from https://advanced.onlinelibrary.wiley.com/doi/10.1002/advs.202520797 by Spanish Cochrane National Provision (Ministerio de Sanidad), Wiley Online Library on [24/04/2026]. See the Terms and Conditions (https://onlinelibrary.wiley.com/terms-and-conditions) on Wiley Online Library for rules of use; OA articles are governed by the applicable Creative Commons License

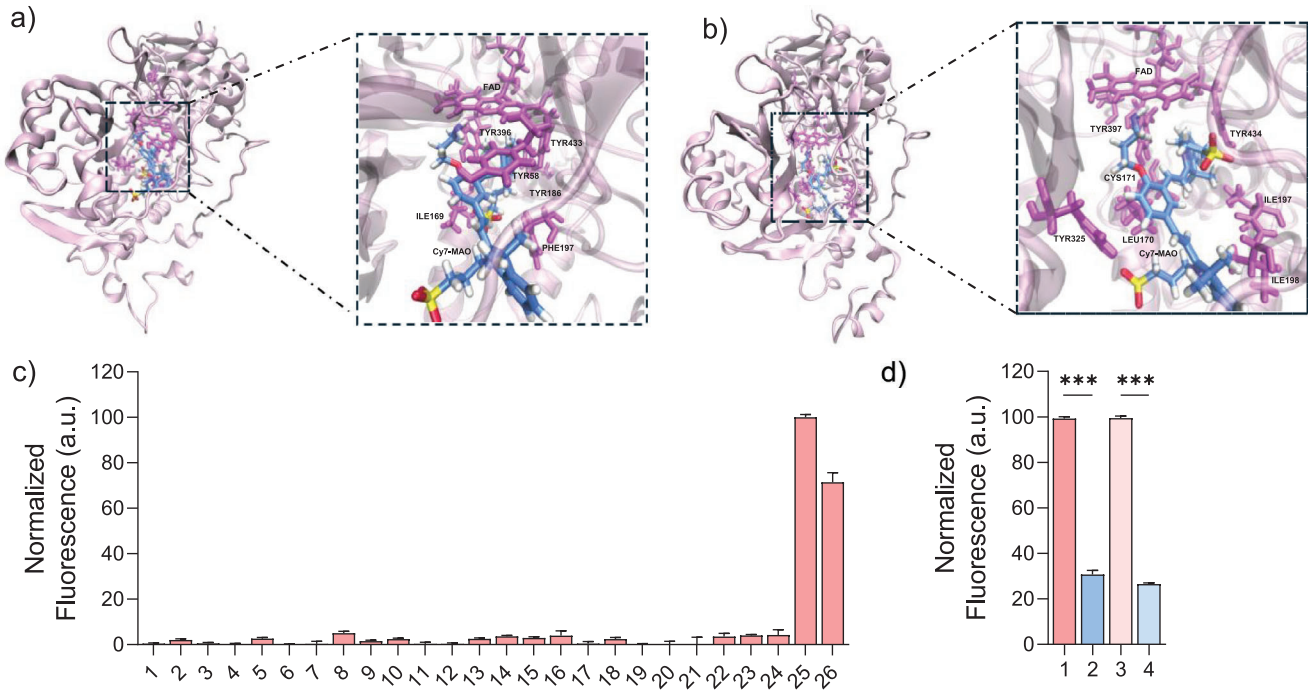


FIGURE 4 | Molecular docking and selectivity studies. Interaction of **Cy7-MAO** with isozymes MAO-A and MAO-B. (a) The MAO-A enzyme is depicted in Cartoon form, and the active site residues are displayed in stick form. **Cy7-MAO** (blue) is buried in the substrate binding pocket of the protein. The substrate binding residues are in the form of sticks (purple) and are labeled for a better illustration. (b) The MAO-B enzyme is depicted in Cartoon form, and the active site residues are displayed in stick form. **Cy7-MAO** (blue) is buried in the substrate binding pocket of the protein. The substrate binding residues are in the form of sticks (purple) and are labelled for a better illustration. (c) Fluorescence emission of **Cy7-MAO** (5 μM) in HEPES (10 mM, pH=7.4, 37°C) in the presence of different potential interferents at 535 nm (excitation at 450 nm): 1, Na^+ (1 mM); 2, K^+ and NO_3^- (1 mM); 3, Ca^{2+} (1 mM); 4, Mg^{2+} (1 mM); 5, Fe^{2+} (0.2 mM); 6, Fe^{3+} (0.2 mM); 7, H_2O_2 (10 mM); 8, t-BuOOH (100 μM); 9, Vitamin C (1 mM); 10, Glutathione (1 mM); 11, Arginine (1 mM); 12, L-Histidine (1 mM); 13, L-Glutamic acid (1 mM); 14, Urea (20 mM); 15, Glucose (10 mM); 16, BSA (500 μM); 17, Lysozyme (150 $mg{\cdot}mL^{-1}$); 18, Acetyl Cholinesterase (150 $mg{\cdot}mL^{-1}$); 19, Leucine Aminopeptidase (150 $mg{\cdot}mL^{-1}$); 20, β-Galactosidase (150 $mg{\cdot}mL^{-1}$); 21, Phosphatase (150 $mg{\cdot}mL^{-1}$); 22, Esterase (150 $mg{\cdot}mL^{-1}$); 23, DNase (150 $mg{\cdot}mL^{-1}$); 24, Glucose Oxidase (150 $mg{\cdot}mL^{-1}$); 25, MAO-A (100 $\mu g{\cdot}mL^{-1}$) and 26, MAO-B (100 $\mu g{\cdot}mL^{-1}$). (d) Fluorescence intensity: 1: **Cy7-MAO** + MAO-A; 2: **Cy7-MAO** + MAO-A + CL (clorgyline, a specific MAO-A inhibitor); 3: **Cy7-MAO** + MAO-B; 4: **Cy7-MAO** + MAO-B + PA (pargyline, a specific MAO-B inhibitor). The solutions used were prepared in HEPES (10 mM, pH=7.4, 37°C) with the following concentrations: **Cy7-MAO** (10 μM), MAO-A/B (10 μM), CL, and PA (10 μM). Error bars are expressed as 3σ for three independent experiments. Values are expressed as mean ± SD. Statistical analysis was assessed by applying Student's *t*-test (***$p < 0.001$).

confirming the proposed mechanism; i.e., the emission enhancement is due to the hydrolysis of **Cy7-MAO** by MAO enzymes (Figure 4d).

2.3 | In vitro Validation of the Cy7-MAO Probe

For in vitro validation, human-derived HepG2 (hepatocellular carcinoma) cells were selected for their known overexpression of both MAO isoforms [46]. Initially, **Cy7-MAO** toxicity was tested in HepG2 cells, showing no toxic effect after 48 h of incubation, even at concentrations as high as 200 μM (Figure 5a). Western blot confirmed MAO expression in HepG2, showing endogenous high levels of MAO-A and MAO-B (Figure 5b). In contrast, SK-Mel-103 melanoma human-derived cells, chosen as a negative control, showed minimal levels of MAO-A and MAO-B enzymes (Figure 5b). Confocal images of cells incubated with **Cy7-MAO** probe showed a strong fluorescence signal in HepG2 cells compared to SK-Mel-103 cells (Figure 5c,d). These results confirm the selective hydrolysis of **Cy7-MAO** in HepG2, supporting the MAO-dependent activation of the probe in vitro.

2.4 | In vivo Validation of Cy7-MAO Probe

The fact that MAO-A and/or MAO-B enzyme levels are frequently elevated with age has drawn attention to their potential contribution of MAO enzymes to physiological aging. Accumulating evidence indicates that MAO enzyme levels rise with age in various tissues, including the brain and liver, contributing to increased ROS production and mitochondrial dysfunction [47, 48]. These processes are considered key mechanisms in physiological aging and age-related pathologies [49]. Given this established relationship, we were interested in evaluating the ability of **Cy7-MAO** for non-invasive readout of MAO in the context of aging. To this end, we conducted two complementary in vivo experiments using BALB/cByJ mice. In the first experiment, focused on mechanistic validation of the probe, we performed a comparative analysis between two distinct age groups, young (2 months) and aged (12 months), to explore functionality and specificity of the probe in detecting age-dependent MAO differences. Mice were intraperitoneally administered with 10 mM **Cy7-MAO**, and the fluorescence emission was monitored by IVIS (In Vivo Imaging System) technique (Figure 6a). In vivo IVIS imaging after 15 min showed a fluorescent signal around the peritoneal area and

21983844, 2026, 23, Downloaded from https://advanced.onlinelibrary.wiley.com/doi/10.1002/advs.202520797 by Spanish Cochrane National Provision (Ministerio de Sanidad), Wiley Online Library on [24/04/2026]. See the Terms and Conditions (https://onlinelibrary.wiley.com/terms-and-conditions) on Wiley Online Library for rules of use; OA articles are governed by the applicable Creative Commons License

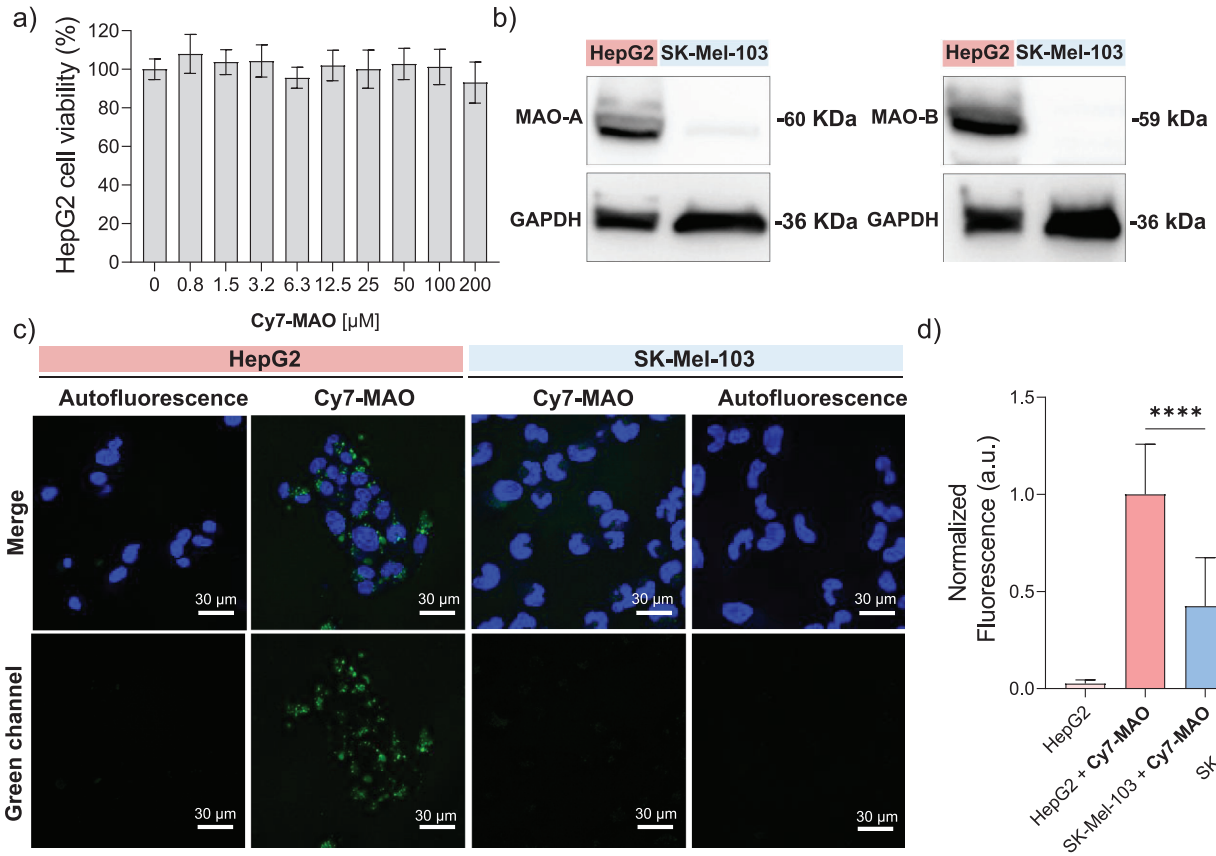


FIGURE 5 | In vitro validation of **Cy7-MAO** probe. (a) Cell viability in HepG2 cells incubated with different concentrations of **Cy7-MAO** probe for 48 h. (b) Western blot assay for MAO-A/B expression in HepG2 and SK-Mel-103 cells. The values are expressed as mean ± SEM ($n = 3$). (c) Confocal images of HepG2 (high endogenous expression of MAO) vs. SK-Mel-103 (control cells) incubated with **Cy7-MAO** (100 μM) for 2 h. Nuclei were stained with Hoechst 33342 (blue channel). Scaler bar: 30 μm. (d) Fluorescence quantification of confocal images. Images show a 2-fold emission enhancement in HepG2 cells when compared with SK-Mel-103 cells. The results exhibited representative images from three independent studies ($n = 3$), and values are expressed as mean ± SD. Statistical analysis was assessed by applying Student's *t*-test (****$p < 0.0001$).

the anatomical region corresponding to the bladder in the older mice injected with **Cy7-MAO** (Figure 6b). For quantification purposes, this specific region of interest (ROI), corresponding to the bladder zone, was consistently used across all animals to assess the relative fluorescence signal (Figure 6c), confirming the elevated fluorescence intensity in older mice. This pattern reflects the design of **Cy7-MAO** as a renal-clearable activatable probe: upon MAO-dependent activation, the fluorescent Cy7 product is rapidly filtered by the kidneys and transiently concentrated in the bladder prior to urine elimination.

After urine collection and euthanasia, the fluorescence of the main organs was studied by IVIS imaging. The strong signal in the bladder of aged animals, compared to young mice (negligible signal), also reflects that **Cy7-MAO** activation occurs in vivo in an age-dependent manner, with fluorescence in the bladder reflecting efficient clearance of the processed probe via the renal pathway (Figure 6d). Moreover, fluorescence readout of urine, collected after mice recovered from anesthesia, correlates with this outcome. Urine samples were collected 15 min after intraperitoneal administration of the **Cy7-MAO** probe and analysed at this reduced time interval to specifically evaluate the fluorescence of the Cy7 fluorophore. Aged mice showed a 5.8-fold increase in urine fluorescence emission from fluorimeter measurements compared to young mice (Figure 6e,f), consistent with higher in vivo **Cy7-MAO** activation. Overall, these findings indicate that **Cy7-MAO** is preferentially activated in aged animals, suggesting that the observed urinary fluorescence reflects age-dependent increases in MAO. To corroborate that, we characterised *Maoa* and *Maob* mRNA levels in brain, lungs, liver, kidneys, and spleen by RT-qPCR in 2 and 12-month-old mice, which serve as a proxy for enzyme expression. Previous studies using quantitative enzyme radioautography in BL6/C57 mice have reported organ-specific, age –related changes in MAO [50]. In our experiments, a significant age-dependent increase in both isoforms was observed in the liver, with *Maoa* and *Maob* levels rising approximately 4.5- and 4-fold in 12-month old mice, respectively (Figure 6g; Figure S16). In contrast, MAO expression remained unchanged in the other examined organs, except for kidneys, which also showed some slight increase in *Maoa*, and specially in *Maob*, levels in 12-month-old mice. In contrast, young mice showed no significant changes in MAO expression across these organs. These results corroborate that the elevated urinary fluorescence observed in aged mice reflects biologically relevant specific increases in MAO expression (both isoforms), while young mice do not exhibit such activation. Although MAO overexpression was widely associated with the brain, particularly in the context of neurodegenerative conditions, its expression in this tissue is known to be variable

21983844, 2026, 23, Downloaded from https://advanced.onlinelibrary.wiley.com/doi/10.1002/advs.202520797 by Spanish Cochrane National Provision (Ministerio de Sanidad), Wiley Online Library on [24/04/2026]. See the Terms and Conditions (https://onlinelibrary.wiley.com/terms-and-conditions) on Wiley Online Library for rules of use; OA articles are governed by the applicable Creative Commons License

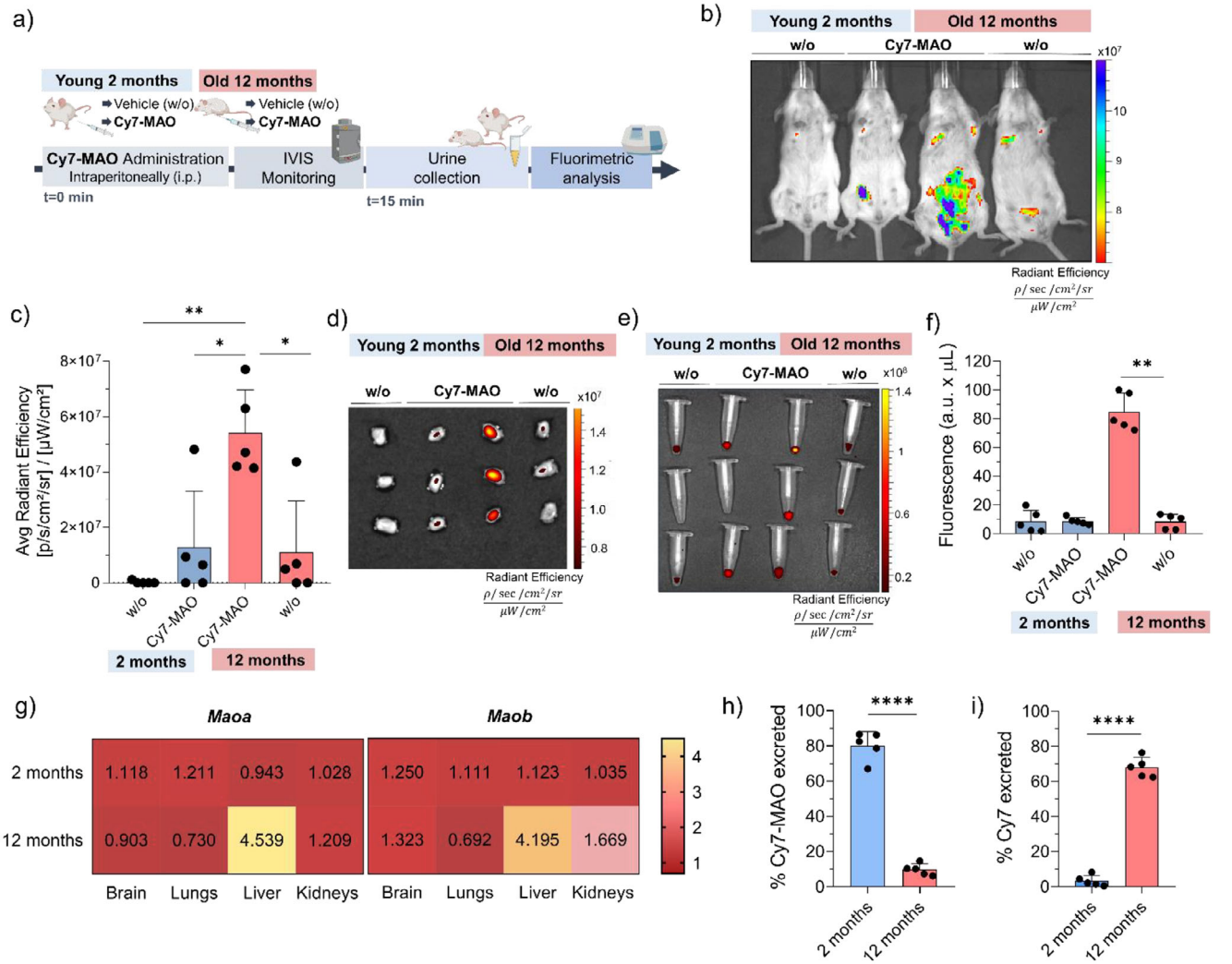


FIGURE 6 | In vivo validation of **Cy7-MAO** probe in a naturally aged mouse model. (a) Timeline for the in vivo evaluation of **Cy7-MAO** probe in naturally aged BALB/cByJ mice model (2- and 12-month mice, $n = 5$ animals per group). (b) Representative IVIS images of BALB/cByJ mice i.p injected with **Cy7-MAO** and (c) quantification. (d) Ex vivo IVIS image of bladder from young (2 months) and old (12 months) after **Cy7-MAO** or vehicle treatment (w/o). The image shows that only the bladder from old mice treated with **Cy7-MAO** exhibits a strong fluorescence signal. (e) Representative IVIS image of urine samples from young (2-month) and old (12-month) mice recorded 15 min after **Cy7-MAO** or vehicle treatment (w/o). (f) Fluorimeter measurement of Cy7 fluorophore in the urine of BALB/cByJ mice of different ages. Fluorescence values were normalized considering total urine volume (a.u. x mL) to avoid variability in micturition and ensure accurate comparison between groups. The values are expressed as mean ± SD. Statistical significance was assessed by the one-way ANOVA followed by a Tukey's test: ****$p < 0.0001$. (g) Heat map of MAO expression in main organs corroborated by real-time qPCR. Values represent the mean of relative MAO mRNA expression ($n = 5$). *Actb* (β-actin) was used for input normalization. (h) **Cy7-MAO** (%) and (i) Cy7 (%) excreted through urine from BALB/c mice measured by HPLC-MS. Values are expressed as mean ± SD. Statistical analysis was assessed by applying one-way followed by a Tukey's test: ****$p < 0.0001$.

and context dependent [51]. On the other hand, our observations align with previous studies suggesting the liver as a major site of peripheral MAO activity in aging [52, 53, 25]. This enzymatic upregulation is consistent with reported age-related hepatic alterations. This can be associated with the elevated oxidative stress and impaired metabolic capacity of the liver relative to other organs. This can lead to chronic inflammation, fibrosis, and increased expression of ROS–generating enzymes such as MAO.

Consistent with this, HPLC-MS analysis performed on urine collected 15 min after probe administration confirmed activation of **Cy7-MAO,** directly linking probe processing to the biological target and demonstrating efficient renal elimination of the activated product. In aged mice (12 months old), approximately 69.6 ± 5.7% of the administered dose of **Cy7-MAO** (38 mg/kg) was recovered in the urine as the Cy7 fluorophore, while 4.1 ± 3.3 % remained as unprocessed **Cy7-MAO** probe (Figure 6h,i). In contrast, in young mice (2 months old), excretion of the Cy7 fluorophore was minimal (ca. 1.5 ± 1.0%), whereas the **Cy7-MAO** probe accounted for approximately 80.1 ± 8.1%. These percentages were calculated by relating the amounts of probe and fluorophore detected in urine to the total dose of **Cy7-MAO** initially administered, reflecting rapid MAO-mediated activation followed by renal clearance. These results confirm that **Cy7-MAO** functions as designed, being selectively activated only in the presence of MAO in aged mice and rapidly cleared with high efficiency

21983844, 2026, 23, Downloaded from https://advanced.onlinelibrary.wiley.com/doi/10.1002/advs.202520797 by Spanish Cochrane National Provision (Ministerio de Sanidad), Wiley Online Library on [24/04/2026]. See the Terms and Conditions (https://onlinelibrary.wiley.com/terms-and-conditions) on Wiley Online Library for rules of use; OA articles are governed by the applicable Creative Commons License

providing a robust, non-invasive readout of age-associated MAO expression. The remaining fraction likely represents transient circulation or distribution in non-target tissues, without affecting probe specificity or reliability of the urinary readout.

In a complementary study, a more detailed functional distribution analysis in aged mice was performed. In vivo imaging monitoring showed the dynamic transit of the probe from the injection site to the urinary system over 0–20 min (Figure 7a). Quantification of the in vivo fluorescence signal showed a clear increase in the bladder region, reflecting the high local concentration of the activated Cy7 fluorophore (Figure 7b). In vivo imaging was performed before urine collection, which is consistent with a high concentration of the activated Cy7 in the bladder. Ex vivo imaging (Figure 7c), performed after urine collection (Figure 7e,f), revealed a portion of residual fluorescence predominantly in the liver and in the bladder with negligible signal in other organs. These patterns do not reflect accumulation or a conventional biodistribution but rather confirm that the activated probe is efficiently cleared via urine, with residual signals arising from sites of enzymatic activation (e.g., liver) or incomplete urinary elimination. The results are consistent with the design of **Cy7-MAO** as a renal-clearable activatable probe: upon MAO-dependent activation, the fluorescent Cy7 product is rapidly processed by the renal system, and temporarily concentrated in the bladder prior to urine elimination. Importantly, acute toxicity studies in healthy mice indicated no detectable adverse effects on well-being, blood chemistry, or organ histology, supporting the biocompatibility of the probe at the tested dose (Figure S17).

To further investigate whether **Cy7-*MAO*** could detect more gradual, age-associated changes in MAO activity and support longitudinal studies, a second experiment was carried out with mice at intermediate ages. Specifically, BALB/cByJ mice aged 2 ($n = 3$), 5 ($n = 3$), 8 ($n = 3$), and 14 ($n = 2$) months were intraperitoneally administered with **Cy7-MAO** (10 mM), and the urine was collected 15 min after the mice recovered from anesthesia for fluorescence analysis (Figure 7a).

Urine fluorescence measurements revealed an increasing trend in fluorophore emission with mice age (Figure 8b,c). As described above, given the short post-injection interval (15 min), the fluorescence signal corresponds to the formation of the Cy7 fluorophore and not to the hemiCy7 derivative. A significant difference was observed in the emission intensity between the youngest (2-month-old) and the oldest (14-month-old) mice (ca. 6.5-fold), with intermediate values for mice aged 5 and 8 months. These results suggest that **Cy7-MAO** is sufficiently sensitive to detect age-associated differences in MAO levels through urinary fluorescence. HPLC-MS analysis in urine revealed values of Cy7 fluorophore that increased with age from 1.5 ± 0.5% for 2-month-old mice to 62.7 ± 7.1 % for 14-month-old mice (Figure 8d). HPLC-MS analysis also demonstrated that the remaining **Cy7-MAO** probe that is not hydrolysed is also excreted through the urine with values ranging from 76.4 ± 5.9% to 8.2 ± 5.7 % of the injected probe for 2- and 14-month-old mice (Figure 8e). Intermediate age groups (5 and 8 months) showed progressive increases of Cy7, and a decrease of **Cy7-MAO** compared to 2-month-old mice. These observations are consistent with the fact that younger animals, which exhibit lower MAO enzymatic activity, excrete a larger proportion of the **Cy7-MAO** probe. In contrast, older animals, with higher MAO activity, show extensive conversion of **Cy7-MAO** into the fluorescent Cy7 product. This age-dependent differential activation provides a clear dynamic window, demonstrating that the probe can effectively discriminate variations in MAO activity across different ages. As in the previous study, these data indicate that a large amount of the injected probe is eliminated in the urine (as Cy7 or **Cy7-MAO**) after only 15 min, suggesting minimal retention in tissues or elimination via alternative pathways, and confirming renal excretion as the main clearance route. Additionally, to further confirm the physiological aging context in the liver as suggested in the study above, hepatic expression levels of the senescence marker $p16^{Ink4a}$ (encoded by the *Cdkn2a* gene) were evaluated across the different age groups. A progressive increase in *Cdkn2a* levels was observed with age, with a marked expression in 14-month-old mice (Figure 8f), thereby linking the observed **Cy7-MAO** activation to an aging phenotype. Overall, these results corroborate the potential of the **Cy7-MAO** probe as a minimally invasive tool for detecting biologically relevant MAO-dependent differences in aging, offering complementary insights beyond static gene expression assays.

Inspired by the above results, the **Cy7-MAO** probe was also validated in additional mouse models of different ages, such as the senescence-prone SAMP8 (2 and 8 months) [54] and the naturally aging C57BL/6 strain (2 and 16 months) (Figure 8g), following a similar procedure to that described above. Urine analysis revealed a significant increase in fluorescence emission with age in both strains. Specifically, an approximately 2.2-fold increase in fluorescence intensity was observed between 2- and 8-month-old SAMP8 mice (Figure 8h), and a 2.8-fold increase was detected between 2- and 16-month-old C57BL/6 mice (Figure 8i). These findings indicate that the age-related increase in MAO is consistent across different mouse strains and observed in both natural (BALB/cByJ and C57BL/6) and accelerated aging (SAMP8) models, highlighting the versatility of **Cy7-MAO** as a tool for detecting MAO-dependent changes in vivo with age.

Overall, these results demonstrate the potential use of the **Cy7-MAO** as a reliable and non-invasive fluorescent probe for monitoring MAO activity in vivo, as evidenced by the clear correlation between age-related increases in MAO activity and urinary fluorescence.

3 | Conclusions

In the context of precision medicine, one attractive approach is to detect biomarkers from accessible biofluids using simple detection systems to guide healthcare decisions. One approach toward this aim is the design of probes in an OFF state that can be transformed by specific biomarkers in cells or tissues in vivo to give an ON, highly emissive product that can be renally cleared, allowing fluorescence detection in urine by simple techniques. Based on this concept, we report herein a fluorogenic molecular probe (**Cy7-MAO**) to selectively detect MAO enzymes through fluorescence measurements in collected urine samples. MAO enzymes induce the oxidative deamination of the poorly fluorescent **Cy7-MAO** probe, generating the highly emissive Cy7 fluorophore, which evolves with time to the also emissive hemiCy7. Confocal studies confirmed the ability of **Cy7-MAO** to

21983844, 2026, 23, Downloaded from https://advanced.onlinelibrary.wiley.com/doi/10.1002/advs.202520797 by Spanish Cochrane National Provision (Ministerio de Sanidad), Wiley Online Library on [24/04/2026]. See the Terms and Conditions (https://onlinelibrary.wiley.com/terms-and-conditions) on Wiley Online Library for rules of use; OA articles are governed by the applicable Creative Commons License

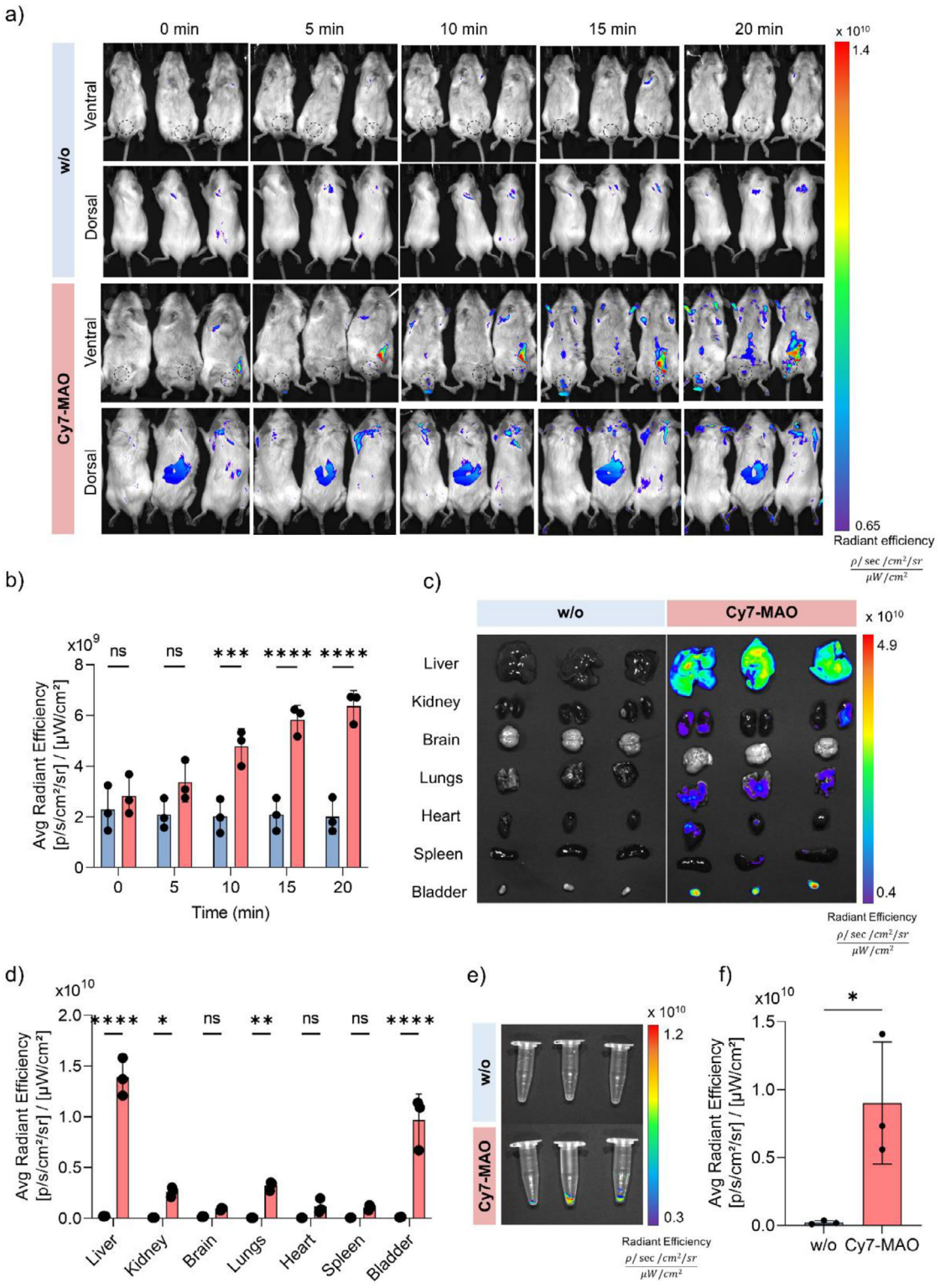


FIGURE 7 | Functional distribution analysis of **Cy7-MAO** in naturally aged mice. (a) AniView Phoenix obtained images of **Cy7-MAO** (12-month-old) and vehicle-treated mice after 0, 5, 10, 15, and 20 min in dorsal and ventral position. (b) Fluorescence (avg. Radiant effiency) quantification of bladder region in ventral images at different times. Images were taken before urine collection. (c) Ex vivo AniView Phoenix images and (d) quantification of dissected tissue of **Cy7-MAO** (12-month-old) (pink bars) or vehicle (blue bars) treatment after 15 min and quantification. Ex vivo images were taken after urine collection. Data is represented as mean ± SD ($n = 3$). Statistical significance was assessed by applying two-way ANOVA followed by a multiple-comparison test. (e) AniView Phoenix images and (f) fluorescence quantification of urine collected from mice injected with **Cy7-MAO** (pink bars) or vehicle (blue bars). Data is represented as mean ± SD ($n = 3$). Statistical significance was assessed by applying unpaired t-test: $^*p < 0.05$.

21983844, 2026, 23, Downloaded from https://advanced.onlinelibrary.wiley.com/doi/10.1002/advs.202520797 by Spanish Cochrane National Provision (Ministerio de Sanidad), Wiley Online Library on [24/04/2026]. See the Terms and Conditions (https://onlinelibrary.wiley.com/terms-and-conditions) on Wiley Online Library for rules of use; OA articles are governed by the applicable Creative Commons License

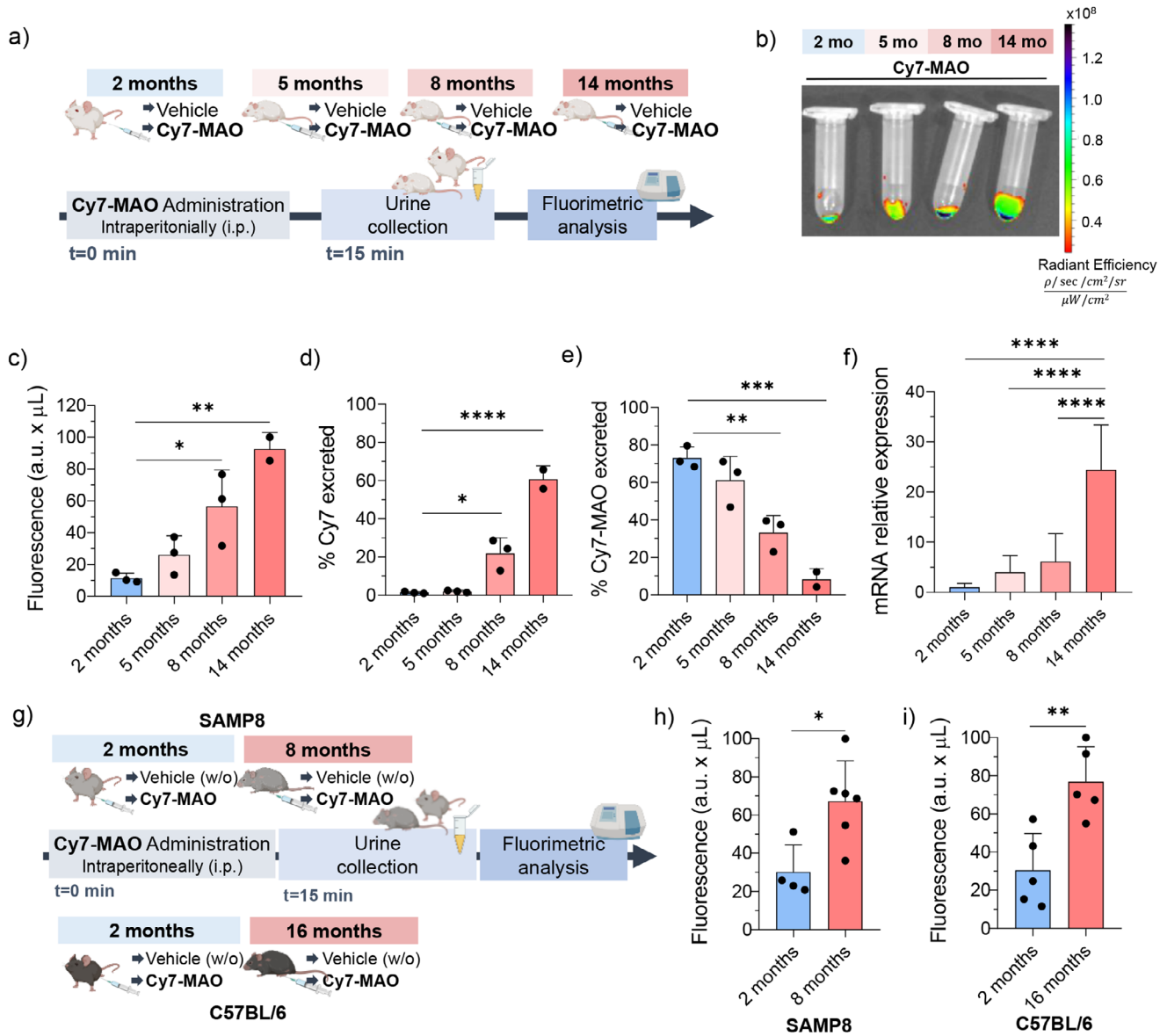


FIGURE 8 | In vivo validation of **Cy7-MAO** probe across aging progression and mouse models. (a) Timeline for the in vivo evaluation of **Cy7-MAO** probe in naturally aged BALB/cByJ mice. (b) Representative IVIS image of urine samples from 2-, 5-, 8-, and 14-months mice recorded 15 min after **Cy7-MAO**. (c) Fluorimeter measurement of Cy7 fluorophore in the urine of BALB/cByJ mice of different ages. Fluorescence values were normalized considering total urine volume (a.u. x mL) to avoid variability in micturition and ensure accurate comparison between groups. The values are expressed as mean ± SD. Statistical significance was assessed by the one-way ANOVA followed by a Tukey's test: $^{**}p < 0.01$. (d) Measurement of the percentage of Cy7 fluorophore excreted in the urine by HPLC-MS. The values are expressed as mean ± SD. Statistical significance was assessed by the one-way ANOVA followed by a Tukey's test: $^{****}p < 0.0001$. (e) Measurement of the percentage of **Cy7-MAO** probe excreted in the urine by HPLC-MS. The values are expressed as mean ± SD. Statistical significance was assessed by the one-way ANOVA followed by a Tukey's test: $^{***}p < 0.001$. (f) mRNA expression levels of *Maoa* of *Cdkn2a* (which encodes for $p16^{Ink4a}$) in liver corroborated by real-time PCR. *Actb* was used for input normalization. Values are relative to control mice and are expressed as mean ± SD. Statistical significance was assessed by the one-way ANOVA followed by a Tukey's test: $^{*}p < 0.05$; $^{**}p < 0.01$; $^{***}p < 0.001$; $^{****}p < 0.0001$ ($n = 3$). (g) Timeline for the in vivo evaluation of **Cy7-MAO** probe in SAMP8 and C57BL/6 mice. (h) Fluorimeter measurement of Cy7 fluorophore in the urine of SAMP8 and (i) C57BL/6 mice of different ages. Fluorescence values were normalized considering total urine volume (a.u. x mL) to avoid variability in micturition and ensure accurate comparison between groups. The values are expressed as mean ± SD. Statistical significance was assessed by the one-way ANOVA followed by a Tukey's test, $^{*}p < 0.05$; $^{**}p < 0.01$.

detect MAO in vitro in HepG2, in which there is an endogenous MAO overexpression. We also provided evidence that urinary fluorescence correlates with relative levels of MAO in elderly and young BALB/c mice in vivo. We found that urine emission in 12-month-old mice was 5.8-fold higher than in 2-month-old animals. These are directly related to the relative mRNA expression of *Maoa* and *Maob*, clearly higher in the liver of old mice. Importantly, biodistribution analysis confirmed that after injection, the probe transits through the liver and kidneys to the bladder, with urinary excretion as the main clearance route, and minimal fluorescence was detected in other major organs. This supports the conclusion that urinary fluorescence predominantly

21983844, 2026, 23, Downloaded from https://advanced.onlinelibrary.wiley.com/doi/10.1002/advs.202520797 by Spanish Cochrane National Provision (Ministerio de Sanidad), Wiley Online Library on [24/04/2026]. See the Terms and Conditions (https://onlinelibrary.wiley.com/terms-and-conditions) on Wiley Online Library for rules of use; OA articles are governed by the applicable Creative Commons License

reflects liver-associated MAO activity. Additionally, **Cy7-MAO** also captured gradual age-associated changes in MAO levels through urinary fluorescence in BALB/c mice of different ages. A progressive increase in *Cdkn2a* levels was also observed with age, thereby linking the observed **Cy7-MAO** activation to an aging phenotype. Furthermore, validation in additional mouse strains (SAMP8 and C57BL/6) confirmed that this age-associated increase in fluorescence is consistent across genetic backgrounds, supporting the broader applicability of the probe. Overall, the results highlight the value of **Cy7-MAO** as a non-invasive tool to monitor biologically relevant, MAO-dependent changes in aging in vivo, previously not feasible with existing methods. This probe provides a simple and effective readout of MAO-associated alterations, offering a new approach for studying conditions associated with elevated MAO levels and opening the way to linking MAO to its involvement in possible pathological contexts with age. This approach not only provides a simple and effective readout of MAO dysregulation but also underscores the broader applicability of renal-clearable probes for the real-time assessment of multiple metabolic and pathological conditions.

Acknowledgements

This research was supported by projects PID2021-126304OB-C41, PID2021-128141OB-C22, and PID2024-155683OB-C41, funded by MCIN/AEI/10.13039/501100011033/and by European Regional Development Fund—A way of doing Europe, and CIPROM/2021/007, funded by Generalitat Valenciana (GVA), to R. M-M., and PID2020-117937GB-I00 to I.F. The authors acknowledge the financial support from the FEDER found of the European Union (IDIFEDER/2021/044). This research also was supported by CIBER-Consorcio Centro de Investigación Biomédica en Red-(CB06/01/2012 and CB06/05/0086), Instituto de Salud Carlos III, MCIN. This study was also supported by the project PAID-06-24 funded by Universitat Politècnica de València. J. F. B. thanks the support from the "la Caixa" Foundation (ID 100010434) under the fellowship code LCF/BQ/PR24/12050022. D. A. -S. thanks his predoctoral fellowship CIACIF from GVA (CIACIF/2022/132). J. G. -F. thanks his predoctoral fellowship GRISOLIA from GVA (GRISOLIAP/2021/122) A.G-F. thanks the Instituto de Salud Carlos III and the European Social Fund for financial support "Miguel Servet" (CP25/00067).

Conflicts of Interest

The authors declare no conflicts of interest.

Data Availability Statement

The data that support the findings of this study are available from the corresponding author upon reasonable request.

References

1. P. Cheng and K. Pu, "Molecular Imaging And Disease Theranostics With Renal-Clearable Optical Agents," *Nature Reviews Materials* 6 (2021): 1095–1113.

2. R. C. Fitzgerald, A. C. Antoniou, L. Fruk, and N. Rosenfeld, "The Future Of Early Cancer Detection," *Nature Medicine* 28 (2022): 666–677.

3. E. Brown, J. Brunker, and S. E. Bohndiek, "Photoacoustic Imaging As A Tool To Probe The Tumour Microenvironment," *Disease Models & Mechanisms* 2019, 12, dmm039636.

4. S. Siddique and J. C. Chow, "Application of Nanomaterials in Biomedical Imaging and Cancer Therapy," *Nanomaterials* 10 (2020): 1700.

5. S. Rojas-Vázquez, B. Lozano-Torres, A. García-Fernández, et al., "A Renal Clearable Fluorogenic Probe For In Vivo β-Galactosidase Activity Detection During Aging And Senolysis," *Nature Communications* 15 (2024): 775.

6. M. Domínguez, A. García-Fernández, V. Martí-Centelles, F. Sancenón, J. F. Blandez, and R. Martínez-Máñez, "Renal-Clearable Probes For Disease Detection And Monitoring," *Trends in Biotechnology* 43 (2024): 1286–1301.

7. J. Huang, J. Li, Y. Lyu, Q. Miao, and K. Puet, "Molecular Optical Imaging Probes For Early Diagnosis Of Drug-Induced Acute Kidney Injury," *Nature Materials* 18 (2019): 1133–1143.

8. G. A. Kwong, G. von Maltzahn, G. Murugappan, et al., "Mass-Encoded Synthetic Biomarkers For Multiplexed Urinary Monitoring Of Disease," *Nature Biotechnology* 31 (2013): 63–71.

9. K. Y. Lin, G. A. Kwong, A. D. Warren, D. K. Wood, and S. N. Bhatia, "Nanoparticles That Sense Thrombin Activity As Synthetic Urinary Biomarkers Of Thrombosis," *ACS Nano* 7 (2013): 9001–9009.

10. J. Huang, J. Li, Y. Lyu, Q. Miao, and K. Pu, "Molecular Optical Imaging Probes For Early Diagnosis Of Drug-Induced Acute Kidney Injury," *Nature Materials* 18 (2019): 1133–1143.

11. H. Choi, W. Liu, P. Misra, et al., "Renal Clearance Of Quantum Dots," *Nature Biotechnology* 25 (2007): 1165–1170.

12. P. Cheng, W. Chen, S. Li, S. He, Q. Miao, and K. Pu, "Fluoro-Photoacoustic Polymeric Renal Reporter for Real-Time Dual Imaging of Acute Kidney Injury," *Advanced Materials* 32 (2020): 1908530.

13. S. S. Liew, Z. Zeng, P. Cheng, H. Sh, Z. Ch, and K. Pu, "Renal-Clearable Molecular Probe for Near-Infrared Fluorescence Imaging and Urinalysis of SARS-CoV-2," *Journal of the American Chemical Society* 143 (2021): 18827–18831.

14. L. G. Iacovino, F. Magnani, and C. Binda, "The Structure Of Monoamine Oxidases: Past, Present, And Future," *Journal of Neural Transmission* 125 (2018): 1567–1579.

15. D. P. M, R. Kettler, H. H. Keller, et al. Neurotransmitter Actions and Interactions: Proceedings of a Satellite Symposium of the 12th International Society for Neurochemistry Meeting, Algarve, (Journal of Neural Transmission. Supplementa #29), (Springer, 1989).

16. X. Wu, W. Shi, X. Li, and H. Ma, "Recognition Moieties of Small Molecular Fluorescent Probes for Bioimaging of Enzymes," *Accounts of Chemical Research* 52 (2019): 1892–1904.

17. J. Huang, D. Hong, W. Lang, et al., "Recent Advances In Reaction-Based Fluorescent Probes For Detecting Monoamine Oxidases In Living Systems," *Analyst* 144 (2019): 3703–3709.

18. H. Qin, L. Li, K. Li, and Y. Xiaoqi, "Novel Strategy Of Constructing Fluorescent Probe For MAO-B Via Cascade Reaction And Its Application In Imaging MAO-B In Human Astrocyte," *Chinese Chemical Letters* 30 (2019): 71–74.

19. M. P. Mattson, "Apoptosis In Neurodegenerative Disorders," *Nature Reviews Molecular Cell Biology* 1 (2000): 120–130.

20. Y. Santin, J. Resta, A. Parini, and J. Mialet-Perez, "Monoamine Oxidases In Age-Associated Diseases: New Perspectives For Old Enzymes," *Ageing Research Reviews* 66 (2021): 1–13.

21. G. E. Janssens, A. C. Meinema, J. Gonzalez, et al., "Protein Biogenesis Machinery Is A Driver Of Replicative Aging In Yeast," *Elife* 4 (2015): 08527.

22. J. C. Shih, K. Chen, and M. J. Ridd, "Monoamine Oxidase: From Genes to Behavior," *Annual Review of Neuroscience* 22 (1999): 197–217.

23. M. B. Youdim, D. Edmondson, and K. F. Tipton, "The Therapeutic Potential Of Monoamine Oxidase Inhibitors," *Nature Reviews Neuroscience* 7 (2006): 295–309.

24. R. Wang, X. Han, J. You, F. Yu, and L. Chen, "Ratiometric Near-Infrared Fluorescent Probe for Synergistic Detection of Monoamine Oxidase B and Its Contribution to Oxidative Stress in Cell and Mice Aging Models," *Analytical Chemistry* 90 (2018): 4054–4061.

21983844, 2026, 23, Downloaded from https://advanced.onlinelibrary.wiley.com/doi/10.1002/advs.202520797 by Spanish Cochrane National Provision (Ministerio de Sanidad), Wiley Online Library on [24/04/2026]. See the Terms and Conditions (https://onlinelibrary.wiley.com/terms-and-conditions) on Wiley Online Library for rules of use; OA articles are governed by the applicable Creative Commons License

25. A. Nicotra, F. Pierucci, H. Parvez, and O. Senatori, "Monoamine Oxidase Expression During Development And Aging," *Neurotoxicology* 25 (2004): 155–165.

26. B. Mathew, E. M. G, J. Suresh, et al., "Monoamine Oxidase Inhibitors: Perspective Design for the Treatment of Depression and Neurological Disorders," *Current Enzyme Inhibition* 12 (2016): 115–122.

27. H. Kunugi and A. Mohammed Al, "Royal Jelly and Its Components Promote Healthy Aging and Longevity: From Animal Models to Humans," *International Journal of Molecular Sciences* 20 (2019): 1–26.

28. M. Cesari, R. Calvani, and E. Marzetti, "Frailty in Older Persons," *Clinics in Geriatric Medicine* 33 (2017): 293–303.

29. F. Y. Pang, F. H. Hucklebridge, G. Forster, K. Tan, and A. Clow, "The Relationship Between Isatin And Monoamine Oxidase-B Inhibitory Activity In Urine," *Stress Medicine* 12 (1996): 35–42.

30. T. Herraiz, A. Flores, and L. Fernández, "Analysis Of Monoamine Oxidase (MAO) Enzymatic Activity By High-Performance Liquid Chromatography-Diode Array Detection Combined With An Assay Of Oxidation With A Peroxidase And Its Application To MAO Inhibitors From Foods And Plants," *Journal of Chromatography B* 1073 (2018): 136–144.

31. G. Huang, F. Zhu, Y. Chen, et al., "A Spectrophotometric Assay For Monoamine Oxidase Activity With 2, 4-Dinitrophenylhydrazine As A Derivatized Reagent," *Analytical Biochemistry* 512 (2016): 18–25.

32. S. B. Edelstein and X. O. Breakefield, "Monoamine Oxidases A And B Are Differentially Regulated By Glucocorticoids And "Aging" In Human Skin Fibroblasts," *Cellular and Molecular Neurobiology* 6 (1986): 121–150.

33. M. Zhou and N. Panchuk-Voloshina, "A One-Step Fluorometric Method for the Continuous Measurement of Monoamine Oxidase Activity," *Analytical Biochemistry* 253 (1997): 169–174.

34. J. Huang, D. Hong, W. Lang, et al., "Recent Advances In Reaction-Based Fluorescent Probes For Detecting Monoamine Oxidases In Living Systems," *The Analyst* 144 (2019): 3703–3709.

35. A. E. Albers, K. A. Rawls, and C. J. Chang, "Activity-Based Fluorescent Reporters For Monoamine Oxidases In Living Cells," *Chemical Communications* 44 (2007): 4647–4649.

36. J. Aw, Q. Shao, Y. Yang, T. Jiang, C. Ang, and B. Xing, "Synthesis and Characterization of 2-(2′-hydroxy-5′-chlorophenyl)-6-chloro-4(3 H)-Quinazolinone-Based Fluorogenic Probes for Cellular Imaging of Monoamine Oxidases," *Chemistry—An Asian Journal* 5 (2010): 1317–1321.

37. L. L. Li, K. Li, Y. H. Liu, H. R. Xu, and X. Q. Yu, "Red Emission Fluorescent Probes For Visualization Of Monoamine Oxidase In Living Cells," *Scientific Reports* 6 (2016): 31217.

38. Z. M. Yang, Q. Y. Mo, J. M. He, et al., "Mitochondrial-Targeted and Near-Infrared Fluorescence Probe for Bioimaging and Evaluating Monoamine Oxidase A Activity in Hepatic Fibrosis," *ACS Sensors* 5 (2020): 943–951.

39. J. Shang, W. Shi, X. Li, and H. Ma, "Water-Soluble Near-Infrared Fluorescent Probes for Specific Detection of Monoamine Oxidase A in Living Biosystems," *Analytical Chemistry* 93 (2021): 4285–4290.

40. J. Wu, C. Han, X. Cao, et al., "Mitochondria Targeting Fluorescent Probe For MAO-A And The Application In The Development Of Drug Candidate For Neuroinflammation," *Analytica Chimica Acta* 1199 (2022): 339573.

41. J. Huang, S. Weinfurter, C. Daniele, et al., "Zwitterionic Near Infrared Fluorescent Agents For Noninvasive Real-Time Transcutaneous Assessment Of Kidney Function," *Chemical Science* 8 (2017): 2652–2660.

42. M. Domínguez, D. Azorín-Soriano, J. García-Fleitas, et al., "Development Of A Novel Near-Infrared Fluorescent Probe Based On Nile Blue For The Detection Of Leucine Aminopeptidase As A Cancer Biomarker," *Dyes and Pigments* 240 (2025): 112827.

43. K. Bondar, M. Bokan, G. Gellerman, and L. D. Patsenker, "Water-Soluble 4-Hydroxystyryl and 4-Hydroxyphenyl-Butadienyls Dyes With Switchable Fluorescence," *Dyes and Pigments* 172 (2020): 107801.

44. M. Bokan, K. Bondar, V. Marks, G. Gellerman, and L. D. Patsenker, "Switchable phenolo-cyanine reporters containing reactive alkylcarboxylic groups for fluorescence-based targeted drug delivery monitoring," *Dyes and Pigments* 159 (2018): 18–27.

45. R. B. Silverman, "Radical Ideas About Monoamine Oxidase," *Accounts of Chemical Research* 28 (1995): 335–342.

46. H. G. Brunner, M. Nelen, X. O. Breakefield, H. H. Ropers, and B. Van Oost, "Abnormal Behavior Associated With a Point Mutation in the Structural Gene for Monoamine Oxidase A," *Science* 262 (1993): 578–580.

47. J. C. Shih and K. Chen, "Regulation of MAO-A and MAO-B Gene Expression," *Current Medicinal Chemistry* 11 (2004): 1995–2005.

48. M. S. Rahman, M. S. Uddin, M. A. Rahman, et al., "Exploring the Role of Monoamine Oxidase Activity in Aging and Alzheimer's Disease," *Current Pharmaceutical Design* 27 (2021): 4017–4029.

49. N. Kaludercic, R. J. Arusei, and L. F. Di, "Recent Advances On The Role Of Monoamine Oxidases In Cardiac Pathophysiology," *Basic Research in Cardiology* 118 (2023): 41.

50. J. Saura, J. G. Richards, and N. Mahy, "Differential Age-Related Changes Of Mao-A And Mao-B In Mouse Brain And Pe Peripheral Organs," *Neurobiology of Aging* 15 (1994): 399–408.

51. T. Behl, D. Kaur, A. Sehgal, et al., "Role of Monoamine Oxidase Activity in Alzheimer's Disease: An Insight Into the Therapeutic Potential of Inhibitors," *Molecules (Basel, Switzerland)* 26 (2021): 3724.

52. F. Yan, X. Tian, Z. Luan, L. Feng, X. Ma, and T. D. James, "NAG-Targeting Fluorescence Based Probe For Precision Diagnosis Of Kidney Injury," *Chemical Communications* 55 (2019): 1955–1958.

53. J. Sholl and S. I. S. Rattan, "Biomarkers of Health and Healthy Ageing from the Outside-In," *Biomarkers of Human Aging* (Springer, 2019).

54. T. Takeda, M. Hosokawa, S. Takeshita, et al., "A New Murine Model Of Accelerated Senescence," *Mechanisms of Ageing and Development* 17 (1981): 183–194.

Supporting Information

Additional supporting information can be found online in the Supporting Information section.

Supporting File: advs74414-sup-0001-SuppMat.docx

21983844, 2026, 23, Downloaded from https://advanced.onlinelibrary.wiley.com/doi/10.1002/advs.202520797 by Spanish Cochrane National Provision (Ministerio de Sanidad), Wiley Online Library on [24/04/2026]. See the Terms and Conditions (https://onlinelibrary.wiley.com/terms-and-conditions) on Wiley Online Library for rules of use; OA articles are governed by the applicable Creative Commons License